1

Quantitative estimation of the impact of European teleconnections on

interannual variation of East Asian winter temperature and monsoon

4

5

Young-Kwon Lim[1] and Hae-Dong Kim[2]

7

[1] NASA Goddard Space Flight Center, Goddard Earth Sciences Technology
and Research (GESTAR), I. M. System Group, Maryland, U.S.A.
(Email: Young-Kwon.Lim@nasa.gov)

11

[2] College of Environment, Keimyung University, Daegu, South Korea
(Email: khd@kmu.ac.kr)

14

15

18

Abstract

The impact of European teleconnections including the East Atlantic/West Russia (EA/WR), the Scandinavia (SCA), and the East Atlantic (EA) on East Asian winter temperature variability was quantified and compared with the combined effect of the Arctic Oscillation (AO), the Western Pacific (WP), and the El-Niño Southern Oscillation (ENSO), which are originated in the Northern Hemispheric high-latitudes or the Pacific. Three European teleconnections explained 22–25% of the total monthly upper-tropospheric height variance over Eurasia. Regression analysis revealed warming by EA/WR and EA and cooling by SCA over mid-latitude East Asia during their positive phase and vice versa. Temperature anomalies were largely explained by the advective temperature change process at the lower troposphere. The average spatial correlation over East Asia (90–180°E, 10–80°N) for the last 34 winters between observed and reconstructed temperature comprised of AO, WP and ENSO effect (AWE) was ~0.55, and adding the European teleconnection components (ESE) to the reconstructed temperature improved the correlation up to ~0.64. Lower level atmospheric structure demonstrated that approximately five of the last 34 winters were significantly better explained by ESE than AWE to determine East Asian seasonal winter temperatures. We also compared the impact between EA/WR and AO on the 1) East Asian winter monsoon, 2) cold surge, and 3) the Siberian high. These three were strongly coupled, and their spatial features and interannual variation were somewhat better explained by EA/WR than AO. Results suggest that the EA/WR impact must be treated more importantly than previously thought for a better understanding of East Asian winter temperature and monsoon variability.

1. Introduction

The impact of planetary-scale circulation patterns (i.e., teleconnection) on East Asian winter temperature variability have been explored in many studies primarily focusing on the Arctic Oscillation (AO) (Jeong and Ho 2005; Park et al. 2011) or El Niño Southern Oscillation (ENSO) (Chen et al. 2004). However, recent studies argue the decreasing role of ENSO (He et al. 2013) and increasing role of other large-scale patterns to influence East Asian winter temperatures. For example, Lim et al. (2012) and Liu et al. (2012) found the importance of the Arctic sea ice variation to drive an anomalously warm or cold winter over East Asian region. Another important factor that possibly affects East Asian winter temperature is the teleconnection patterns originating in the North Atlantic. Several studies have suggested the possible impact of the European teleconnections on East Asian winter climate variability (Bueh and Nakamura 2009; Wang et al. 2011). The East Atlantic/West Russia (EA/WR) (Barnston and Livezey 1987; Washington et al. 2000), Scandinavia (SCA) (Wallace and Gutzler 1981), and East Atlantic (EA) (Bojariu and Reverdin 2002) patterns are examples of European teleconnections suggesting to affect East Asian winter temperatures. However, their importance in determining East Asian winter temperatures has not attracted any significant or detailed investigations. Few studies have critically examined the responsible dynamic mechanism and assessed the significance of their impacts, compared with the relatively well-understood impacts originating from the Pacific (e.g., the Western Pacific (WP) and the ENSO) or the Northern hemispheric high-latitudes (e.g., AO).

The AO is understood to be a dominant teleconnection resolving East Asian winter monsoon (EAWM) variability (Gong et al. 2001; Li and Yang 2010). However, Wang et al.

3

65 (2011) suggested the possible role of EA/WR in modulating EAWM variability. That study

66 found a correlated structure between meridional wind anomalies over East Asia in winter

67 and sea surface temperatures in the preceding summer over the North Atlantic, where the

68 study presumed was the source region for the EA/WR-like teleconnection pattern. We also

69 suggest that the large-scale pressure anomaly in central Russia driven by the EA/WR can

70 affect the EAWM significantly. This pressure pattern is strongly related to the Siberian high,

71 and as commented in Wu and Wang (2002b), this Siberian high may not be necessarily

72 dependent on the AO for influencing the EAWM. It would be worthwhile to compare the

73 strength of the EA/WR impact with the AO impact on East Asian winter temperatures

74 including winter monsoon.

75 The present study was motivated by the lack of understanding of the possible role of

76 European teleconnections in modulating East Asian winter temperatures and monsoon

77 variability. In this study, we intended to clarify whether the European teleconnections are

78 one of the dominant components comprising large-scale climate variability over East Asia.

79 Their impact was then quantitatively estimated through regression, correlation, and a

80 temperature advective process (Linkin and Nigam 2008) to better identify their role in

81 determining anomalous winter temperatures over East Asia. The degree of their

82 contribution to East Asian winter temperature was also compared with the combined effects

83 of AO, WP, and ENSO. Particularly, the impact of EA/WR and AO, respectively, on

84 EAWM activity was compared to better identify their importance to modulate East Asian

85 winter climate variability.

86 Section 2 describes the dataset and analysis method used in this study. Estimation of

87 the impact of European teleconnections and their comparison with the impact of AO, WP

4

88   and ENSO are addressed in Section 3. Section 3 also compares the strength between the

89   impact of EA/WR and AO on EAWM activity and the related cold surge, followed by

90   concluding remarks and discussion in Section 4.

91

92   2. Data and methods

93   The primary analytical methods utilized in this study are the rotated empirical

94   orthogonal function (REOF) technique (Richman 1986) and linear regression. The REOF

95   was applied to upper-tropospheric monthly height archived at the Modern Era

96   Retrospective analysis for Research and Applications (MERRA) reanalysis (Rienecker et

97   al. 2011). The analysis time period covers the past 34 winters from December-February

98   (DJF) 1979/80 through DJF 2012/13. Horizontal resolution of the data is 0.5° (latitude) ×

99   0.6667° (longitude). Lower-level (850 hPa) wind and temperature data were used to

100   investigate the thermal advective process over the East Asian domain. We also used 2

101   meter level MERRA temperature data to compare temperature anomalies induced by the

102   impact of European teleconnections with the observed temperature anomalies. Several

103   indices were used, including the East Asian winter monsoon index (EAWMI) (Jhun and

104   Lee 2004; Li and Yang 2010), the cold surge index (CSI) (Chang et al. 2005) and the

105   Siberian high index (SHI) (Panagiotopoulos et al. 2005) to investigate the impact of

106   EA/WR and AO on interannual variation of EAWM and the cold surge.

107

108   3. Results

109   *a. Impact of European teleconnections*

5

110   Dominant large-scale teleconnection patterns were captured using the upper level (250

111   hPa) geopotential height for the domain that spans Europe and Asia. The monthly

112   climatological cycle of the height field for DJF was removed and the REOF technique was

113   applied to capture the leading teleconnection patterns. Three European teleconnection

114   patterns that show height anomalies over East Asia (left panel in Fig. 1) were identified, as

115   well as patterns originating in the Pacific or the Northern hemispheric high-latitude such as

116   AO (right panel in Fig. 1). Anomalies are plotted on a positive phase basis in Fig. 1. The

117   sum of their percentage variance tended to be sensitive to a slight domain change, but it

118   varied within the range of 45–50%. We compared the principal component (PC) time series

119   with the corresponding teleconnection time series available from the National Center for

120   Environmental   Prediction   (NCEP)/Climate   Prediction   Center   (CPC)

121   (ftp://ftp.cpc.ncep.noaa.gov/wd52dg/data/indices/tele_index.nh)   to   confirm   if

122   teleconnection patterns captured here are reliable. We found that the PC and teleconnection

123   time series are highly correlated (>0.7).

124   The EA/WR pattern in Figure 1a consists of two large-scale anomalies over Europe

125   located in Western Europe and Russia north of the Caspian Sea (Barnston and Livezey

126   1987; Washington et al 2000; Wang et al 2011) and an anomaly over the mid-latitude Asian

127   sector. The pattern appears to have a large-scale wave propagation structure spanning the

128   Atlantic, Europe, western Russia, and East Asia. The positive height anomaly over East

129   Asia north of 40°N with the negative anomaly south of it implies anticyclonic circulation

130   with the easterly anomaly from the Pacific along 35–40°N during the positive phase,

131   whereas the opposite is true for the negative phase.

132   The SCA pattern shows height anomalies of the opposite sign occurring over the

133   Scandinavian Peninsula, and southern and eastern Europe (Fig. 1b) (Wallace and Gutzler

134   1981). In addition to the Scandinavian Peninsula and mid-latitude Europe (Bueh and

135   Nakamura 2007), the anomaly values over continental Asia indicate the possible SCA

136   impact on Asian winter climate variability.

137   Figure 1c shows the EA pattern characterized by strong north-south dipole anomalies

138   over the southern part of Europe (Sáenz et al 2001; Bojariu and Reverdin 2002). A positive

139   anomaly over the western part of continental Asia and a negative anomaly around China

140   and Mongolia are found, though their magnitudes are smaller than those over the Atlantic.

141   The southerly wind anomaly can be dominant along the eastern side of the negative height

142   anomaly over China, transporting a warm air mass to the eastern China, Korea, and Japan

143   during this positive EA phase.

144   Spatial distribution of the AO consists of the zonally symmetric alternating anomalies

145   in the Arctic and the Northern Hemispheric mid-latitudes (Fig. 1d) (Thompson and Wallace

146   1998). It is clear that an easterly anomaly crossing the southern part of Japan and Korea is

147   feasible during the positive phase, whereas the negative phase favors a westerly anomaly

148   along mid-latitude East Asia (30–40°N) that could transport a continental cold air mass to

149   this region.

150   Figure 1e represents the WP pattern (Wallace and Gutzler 1981; Mo and Livezey 1986;

151   Barnston and Livezey 1987) characterized by a north-south dipole of height (or pressure)

152   anomalies over the northwestern Pacific. East Asian winter climate can be influenced by

153   circulation on the western side of these height anomalies. Additionally, the meridional

154   pressure gradient during the WP event can modulate intensity of upper-level westerlies

155 (Linkin and Nigam 2008). The height field associated with ENSO in Fig. 1f exhibits a

156 broad positive height anomaly distribution over the East Asian mid-latitudes (30–50°N) and

157 negative anomaly over the southeastern China during an El Niño episode, whereas the

158 opposite response will be true for the La Niña phase.

159   Actual temperature anomalies associated with each European teleconnection (EA/WR,

160 SCA and EA) were quantitatively estimated by regressing the monthly 2 meter air

161 temperature anomalies onto the monthly teleconnection time series. Figure 2a shows a

162 positive temperature response to the positive EA/WR, spanning Northern China, Mongolia,

163 Russia near Lake Baikal, Korea and Japan, whereas a cold temperature response is true for

164 the negative EA/WR. Specifically, the impact of EA/WR tends to be strong in Russia near

165 Lake Baikal with a temperature magnitude greater than 1K. With the magnitude smaller

166 than 1K, the areas affected by EA/WR with a statistical significance over East Asian mid-

167 latitudes are Korea, Japan and northern China north of 35°N.

168   Figure 2b clearly shows that nearly all Eurasia regions have a negative temperature

169 anomaly during the positive SCA. The SCA impact reaches East Asia including the

170 southeastern part of China. Negative temperature anomalies in the range of −1K−−0.5K are

171 found over northern China, Mongolia, and northern Korea, whereas a negative temperature

172 response smaller than that is distributed over Korea, Japan, and eastern China south of

173 40°N. In contrast, a weak positive temperature response < 0.5K is found over the

174 southeastern part of China.

175   The temperature pattern associated with the positive EA in Fig. 2c demonstrates wide

176 coverage of the EA impact spanning East Asia, as the influence over the Korean Peninsula

177 was suggested in Kim et al. (2012). The sign and magnitude of the anomaly is comparable

178   to that of EA/WR, exhibiting a value greater (less) than 0.5K over the region north (south)

179   of ~40°N.

180   The right panels in Fig. 2 represent the regressed lower-level (850 hPa) temperature

181   advection [K day^{-1}] and circulation associated with each teleconnection. Advective

182   temperature change is calculated by $-V_{Tel} \cdot \nabla T_{Cli}$ (Linkin and Nigam 2008). V_{Tel} represents

183   the regressed horizontal winds related to each teleconnection, whereas T_{Cli} are the monthly

184   climatological temperatures. The contribution of the nonlinear component, $-V_{Tel} \cdot \nabla T_{Tel}$,

185   and the other linear component, $-V_{Cli} \cdot \nabla T_{Tel}$, was ignored because their values are an

186   order of magnitude smaller than $-V_{Tel} \cdot \nabla T_{Cli}$. Figure 2d reveals that an anticyclonic

187   circulation was dominant during the positive EA/WR phase over the mid-latitude East Asia

188   and the western Pacific, where a positive height anomaly is seen in Fig. 1a. Favorable

189   conditions for a southerly wind anomaly developed, leading to a warm advection anomaly

190   over vast areas of East Asia covering Mongolia, China, Korea, and Japan. During the

191   positive SCA, the atmosphere is characterized by cold advection with a relatively weak

192   northerly wind anomaly over East Asia (Fig. 2e). In contrast, warm advection in

193   conjunction with southwesterly anomaly is observed over the southeastern China area with

194   statistical significance. The impact of positive EA is a warming over most of East Asian

195   domain, similar to the impact of a positive EA/WR. Figure 2f reveals that warm advection

196   and a southerly wind anomaly is dominant, linked to the eastern side of negative height

197   anomaly and the western side of the positive height anomaly over East Asia found in Fig.

198   1c.

199   The magnitude of wind vectors over East Asia is generally smaller than those over the

200   Siberian region because East Asia is situated in the far eastern side of the downstream

201 region of European teleconnections, where the eastward wave propagation associated with

202 the teleconnections could likely weaken (Bueh and Nakamura 2007; Wang et al 2011; Lim

203 and Kim 2013). However, wind anomalies appear strong enough to influence winter

204 temperature variability over East Asia, as illustrated in Fig. 2. Note that the temperature

205 anomaly and circulation in the event of the negative teleconnection phase can be

206 understood in an opposite manner. The cooling effect by EA/WR and EA and the warming

207 effect by SCA are feasible during their negative episodes.

208

209 *b. Comparison of the impact of European teleconnections with AO, WP, and ENSO*

210   Figures 1 and 2 strongly demonstrate that East Asian winter temperature variability is

211 determined not only by the combined effect of AO, WP, and ENSO (referred to as AWE),

212 but also by the European teleconnections (referred to as ESE). Here, we reconstructed the

213 three sets of monthly temperature data. One set contains the impacts of both AWE and ESE,

214 another contains the ESE effect only, and the other contains the AWE effect only. Data

215 reconstruction was completed by linear combination of the regressed temperature

216 anomalies and corresponding teleconnection time series. We then calculated the spatial

217 correlation between the reconstructed temperatures and observed temperature anomalies in

218 each year for the domain covering East Asia (90–180°E, 10–80°N). Figure 3a is a time

219 series of the resulting spatial correlation values over all 34 winters. The red line

220 representing the correlation of temperatures due to AWE impact with the observations

221 reveals reasonable reproduction of the observed East Asian winter temperature variability,

222 producing a correlation average of 0.55 over all 34 winters. The blue line representing the

223 ESE impact has a correlation average of 0.51. More critical inspection of these time series

10

224 identified several winters such as 1982–83, 1989–90, 1996–97, 2003–04, 2004–05, 2008–

225 09, and 2011–12 when the observed temperatures were rather poorly reproduced by the

226 AWE impact (see the red line with correlations < ~0.4 for those seven winters). Of these

227 seven winters, observed temperatures during five winters, except 1989–90 and 2008-09,

228 were much better explained when both the AWE and ESE impacts were considered, as the

229 black line reflecting the combined effect of both AWE and ESE revealed improved

230 correlation values for those five winters. The correlation value due to the AWE impact was

231 only 0.04 on average for those five winters and the correlation significantly increased up to

232 0.65 after considering both the AWE and ESE impacts. Over all 34 winters, the time series

233 in black, representing the combined effect of AWE and ESE, improved the correlation

234 average to 0.64 from 0.55, which is the correlation due to the AWE impact only.

235   Figure 3b–3g illustrate that observed temperature distributions (Figs. 3d and 3g) are

236 remarkably better explained by considering both the AWE and ESE impacts for the

237 selected two year cases (1996–97 and 2011–12) mentioned in the previous paragraph

238 (Figures 3b and 3e) rather than considering the AWE impact only. Our analysis for the

239 other winter cases of 1982–83, 2003–04, and 2004–05 support this conclusion (figure not

240 shown). However, the remaining winters (28–29 winters) do not exhibit a significantly

241 greater correlation when both AWE and ESE impacts are considered, compared with

242 considering only the AWE impact, as shown in Fig. 3a (see similar correlation values

243 denoted by black and red for many winter cases). This result indicates that although the

244 ESE impact is important to significantly improve the correlation obtained by considering

245 AWE impact only, that significant improvement does not occur for all years. Many winter

11

246 cases reveal that the observed temperature was reasonably reproduced by AWE impacts

247 without a substantial addition of ESE impacts.

248   Atmospheric structures of lower-level temperature advection and circulation due to the

249 ESE impact (left panel in Fig. 4) and AWE impact (right panel in Fig. 4), respectively, were

250 compared for the three selected winters (1996–97, 2003–04 and 2011–12) to more clearly

251 demonstrate that the ESE impact sometimes play a crucial role in reliably explaining the

252 observed temperature distribution shown in Fig. 3. The spatial distribution of temperature

253 advection by the ESE impact for 1996–97 (Fig. 4a) and 2011–12 (Fig. 4c) better reproduces

254 the observed temperature distribution (Figs. 3d and 3g) than the pattern caused by the AWE

255 impact shown in Figs. 4d and 4f. Specifically, the 2011–12 winter was severely cold (Fig.

256 3g) over East Asia and seemed to be a result of European teleconnections that enhanced

257 cold advection (compare Figs. 4c and 4f). Additionally, the 2003–04 winter was recorded

258 as an anomalously warm winter over East Asia (http://www.ncdc.noaa.gov/temp-and-

259 precip/global-maps.php) and this observational feature was better explained by ESE

260 impacts, as warm advection was found over continental East Asia in Fig. 4b but it was not

261 in Fig. 4e (AWE impacts).

262

263 *c. Impact of teleconnection on East Asian winter monsoon and cold surge*

264   East Asian winter temperature is largely influenced by frequency and intensity of cold

265 surges, which are closely linked to the EAWM. Previous studies have argued a dominant

266 role of AO in determining the EAWM activity and cold surge (Gong et al. 2001; Park et al.

267 2011). Park et al. (2011) also addressed, however, that occurrence of cold surge in the form

268 of wave train was little related to the AO phase, indicating that we still need a clarification

269　whether or not the AO phase is a predominant factor to determine EAWM activity and the

270　cold surge over East Asia. In this section, we compared the impact of AO with the impact

271　of EA/WR on 1) East Asian winter monsoon, 2) the cold surge and 3) the Siberian high to

272　verify if the impact of AO is really the most dominant factor to determine variation in those

273　three features. We first defined the EAWM index (EAWMI) (Fig. 5, red-solid line)

274　following Jhun and Lee (2004) and Li and Yang (2010) based on variations in the upper-

275　level westerly jet over East Asia. We found that those two indices were very highly

276　correlated (r = 0.87). Table 1 shows temporal correlations between teleconnection indices

277　(EA/WR and AO) and EAWMI time series. Negative correlation values indicate a strong

278　EAWM during the negative phase of EA/WR and AO, and vice versa. It is clear that

279　EAWMI has a stronger negative correlation with the EA/WR (−0.59) than with the AO

280　(−0.24). Stronger negative correlations with the EA/WR are also found for the cold surge

281　index (CSI) (Fig. 5, red-dashed line) and the Siberian high index (SHI) (Fig. 5, red-dotted

282　line), which will be discussed in more detail later. Figure 5 shows that all indices (EAWMI,

283　CSI, SHI, −EA/WR and −AO) exhibit upward trends for the periods ~1988/89–2012/13

284　winter. Calculating the correlation after removing this linear upward trend over the ~25

285　winters once again produced a stronger negative correlation with the EA/WR (~−0.35) than

286　with the AO (~-−0.10), which is no longer significant. This low correlation with the AO is

287　consistent with Jhun and Lee (2004) and Wu et al. (2006) who suggested little correlation

288　between AO and EAWM on an interannual time scale.

289　　　Atmospheric spatial patterns regressed onto the EAWMI were calculated and then

290　compared with those regressed onto the negative phase of EA/WR and AO, respectively.

291　Figure 6 clearly shows that strong EAWM over East Asia is characterized by below

292   average temperature (Fig. 6a), northerly flow coming from Siberia and the northwestern

293   Pacific (Fig. 6b), enhanced upper-level westerly in mid-latitudes (~20°–40°N) (Fig. 6c) and

294   upper-level continental convergence and oceanic divergence (Fig. 6d). The spatial

295   distributions of these patterns are quite close to the regressed patterns associated with the

296   negative EA/WR shown in Figs. 7a–c. The temperature distribution in Fig. 6a also

297   significantly resembles the pattern in Fig. 2a multiplied by −1, indicating a strong EAWM

298   during the negative EA/WR and vice versa. Figures 7d–f represents the negative AO impact

299   and exhibit similar spatial distributions to those associated with EAWMI (Fig. 6), but the

300   similarity between them is relatively weaker than that between the negative EA/WR (Figs.

301   7a–c) and EAWMI (Fig. 6). For example, the magnitude of upper level westerly anomalies

302   and their locations shown in Fig. 6c are better explained by Fig. 7b than by Fig. 7e. The

303   pressure distribution with the sea-land contrast and large-scale anomaly centered over

304   Siberia seen in Fig. 6b is better reproduced by Fig. 7a than by Fig. 7d. Upper-level

305   divergent/convergent flow between the Asian continent and the northwestern Pacific, which

306   is a typical characteristic of large-scale monsoon circulation, is also better structured in Fig.

307   7c than in Fig. 7f. These characteristic differences imply a connection between EAWM and

308   EA/WR comparable to or closer than a connection between EAWM and AO. Spatial

309   correlations (90°–150°E and 20°–60°N) in Table 2 clarifies that EAWM activity has closer

310   connection with the phase of EA/WR than with the AO. These results are somewhat

311   different from several studies that argued the most dominant role for AO in determining the

312   EAWM intensity (e.g., Gong et al. 2001; Wu and Wang 2002a). However, Gong et al.

313   (2001) also suggested a significant contribution of the Eurasian teleconnection pattern (e.g.,

314   EA/WR) to better explain the interannual variation of EAWM and the Siberian high.

14

315   EAWM activity is also understood to be an indicator of cold surge activity (Jhun and

316   Lee 2004; Li and Yang 2010). Chang et al. (2005) defined CSI for the South China Sea and

317   southeastern Asia using the meridional wind component. We applied that definition to the

318   mid-latitudes for the domain of 90°–130°E and 40°–60°N, which covers northeastern Asia

319   and the eastern side of Siberian high. The CSI was defined as the area-averaged meridional

320   wind over this spatial domain (Fig. 5, red-dashed line). This region was selected because it

321   is a good pathway for the meridional wind coming from the Northern high-latitudes toward

322   mid-latitude East Asia. Note that merigional wind components were multiplied by −1 so

323   that the CSI value is positive during the cold surge year and vice versa. Regressed patterns

324   associated with the CSI were found to resemble Fig. 6, demonstrating that the EAWM is an

325   indicator of cold surge activity over East Asia (Fig. 8). The temporal correlation between

326   CSI and EAWMI is 0.77. Table 3 clearly demonstrates a stronger relationship between the

327   cold surge and negative EA/WR than with the negative AO, which is a good agreement

328   with the conclusion in Table 2.

329   The reason for the higher correlation between the EAWMI and CSI with the EA/WR

330   than with the AO seems to be associated with a better representation of the Siberian high

331   pressure variation due to the impact of EA/WR than AO. This, in turn, indicates that the

332   Siberian high may not be closely linked to the AO (Wu and Wang 2002b). For confirmation,

333   we calculated the Siberian high index (SHI) following Panagiotopoulos et al. (2005) and

334   Hasanean et al. (2013) and then examined its correlation with the EA/WR and AO,

335   respectively.

336   The temporal correlation between SHI vs. CSI and SHI vs. EAWMI is 0.81 and 0.69,

337   respectively, over the last 34 winters, indicating that the Siberian high is strongly coupled

15

338   with the winter monsoon and cold winters over East Asia (Gong and Ho 2002). The spatial

339   distributions regressed onto SHI shown in Fig. 9 are nearly consistent with the patterns

340   regressed onto EAWMI (Fig. 6). Spatial correlations (90°–150°E and 20°–60°N) between

341   SHI and two teleconnections (EA/WR and AO) shown in Table 4 demonstrate that EA/WR

342   better represents the variation in the Siberian high than that of AO. Cheung et al. (2012)

343   described the dominant role of Ural-Siberian blocking for influencing the EAWM. The

344   pressure pattern associated with the blocking (Fig. 3a in Cheung et al. (2012)) resembled

345   the typical pattern of EA/WR over Russia. Our results support the arguments by several

346   studies that the impact of AO alone does not faithfully explain the variation of Siberian

347   high (Wu and Wang 2002b) and the EAWM activity on an interannual time scale (Jhun and

348   Lee 2004).

349

350   4. Conclusion and discussion

351   We investigated the impacts of European teleconnections (ESE: EA/WR, SCA, and

352   EA) on East Asian winter temperature variability focusing on quantifying their impacts and

353   comparing with the impact of AWE (AO, WP and ENSO). The sum of ESE and AWE

354   explained 45–50% of the total monthly upper-troposphere height variance over Eurasia

355   with 22–25% each. Statistically significant temperature anomalies, which are associated

356   with one standard deviation in each teleconnection time series based on linear regression,

357   were found with a 0.5–1K amplitude over mid-latitude East Asia. We found that these

358   temperature anomalies were largely explained by the advective temperature change process

359   at the lower atmospheric level. Of the last 34 winters, five (1982–83, 1996–97, 2003–04,

16

360 2004–05, and 2011–12) exhibited significantly better reproduction of the observed seasonal

361 temperature anomalies due to the impact of ESE than that by AWE.

362   It appears that ESE's overwhelming impact was often found when the strength of the

363 AO impact was weaker than average. The average amplitude of the AO indices obtained

364 from the NCEP/CPC for those five winters was 0.40 with a maximum of 0.98 (2003–04

365 winter), whereas the average over all 34 winters was 0.90.

366   We also determined that the conventional understanding that AO is the most dominant

367 teleconnection to affect the EAWM may need to be re-evaluated. The comparison between

368 the impact of EA/WR and AO on the EAWM activity, the cold surge and the Siberian high

369 provided consistent results that the EA/WR tends to better represent their interannual

370 variation. The EA/WR modulates the variation in the Siberian high more effectively than

371 that of the AO. As evidenced by correlations and regressed patterns in this study, variations

372 in the Siberian high and corresponding monsoon circulation, which leads to a

373 warmer/colder winter over East Asia, was more accurately reproduced by the EA/WR

374 impact, though the AO impact also explained them reasonably.

375   In this study, the North Atlantic Oscillation (NAO) was also captured as one of the

376 dominant REOF modes over the Eurasian domain. However, we did not consider the NAO

377 because of the very small magnitude of the regressed temperature anomalies over mid-

378 latitude East Asia. This is in agreement with Wang et al. (2005) who addressed regionality

379 of the NAO impact. As a result, no significant temperature anomalies were produced over

380 East Asia. Thus, the NAO contributed little to the interannual temperature variability and

381 spatial correlation discussed in Figure 3. Additionally, the calculated spatial correlations

382 with the EAWMI, CSI and SHI-associated patterns (Table 1 through 4) produced lower

383   correlation coefficients with the NAO (correlations not shown) than with any other

384   teleconnection. Jhun and Lee (2004) and Hong et al. (2008) suggested that the impact of

385   NAO is more related to the decadal-scale East Asian cold extreme variability or EAWM

386   rather than to interannual time-scale variability. Decadal-scale variation was not fully

387   examined in this study due to the limited analysis period. Nonetheless, the evidence

388   presented here indicated that the ESE impact, particularly the EA/WR, needs to be treated

389   more importantly than previously thought for a better understanding of the interannual

390   variations in East Asian winter temperature and monsoon.

391

392   Acknowledgement

395

References

396

397 Barnston, A. G., and R. E. Livezey, 1987: Classification, seasonality and persistence of

398 low-frequency atmospheric circulation patterns. *Mon. Wea. Rev.,* **115,** 1083-1126.

399 Bojariu, R., and G. Reverdin, 2002: Large-scale variability modes of freshwater flux and

400 precipitation over the Atlantic. *Clim. Dyn*., **18,** 369-381.

401 Bueh, C., and H. Nakamura, 2007: Scandinavian pattern and its climate impact. *Quart. J.*

402 *Royal. Meteor. Sci.,* **133,** 2117-2131.

403 Chen, T.-C., W.-R. Huang, and J.-H. Yoon, 2004: Interannual variation of the East Asian

404 cold surge activity. *J. Climate*, **17,** 401-413.

405 Gong, D.-Y., S.-W. Wang, and J.-H. Zhu, 2001: East Asian winter monsoon and Arctic

406 Oscillation. *Geophys. Res. Lett*., **28**, 2073-2076.

Gong, D.-Y., and C.-H. Ho, 2002: Siberian high and climate change over middle to high

latitude Asia. *Theor. App. Climatol*., **72**, 1-9.

407 Hasanean, H. M., M. Almazroui, P. D. Jones, and A. A. Alamoudi, 2013: Siberian high

408 variability and its teleconnectios with tropical circulations and surface air temperature

409 over Saudi Arabia. *Clim. Dyn*., **41**, 2003-2018, doi:10.1007/s00382-012-1657-9.

410 He, S., H. Wang, and J. Liu, 2013: Changes in the relationship between ENSO and Asia-

411 Pacific midlatitude winter atmospheric circulation. *J. Climate*, **26,** 3377-3393.

412 Hong, C.-C., H.-H. Hsu, H.-H. Chia, and C.-Y. Wu, 2008: Decadal relationship between

413 the North Atlantic Oscillation and cold surge frequency in Taiwan. *Geophys. Res. Lett*.,

414 **35,** L24707, doi:10.1029/2008GL034766.

415   Jeong, J.-H., and C.-H. Ho, 2005: Changes in occurrence of cold surges over East Asia in

416   association with Arctic Oscillation. *Geophys. Res. Lett*., **32,** L14704,

417   doi:10.1029/2005GL023024.

418   Jhun, J.-G., and E.-J. Lee, 2004: A new East Asian winter monsoon index and associated

419   characteristics of the winter monsoon. *J. Climate*, **17**, 711-726.

420   Kim, J.-S., S. Jain, and Y.-I. Moon, 2012: Atmospheric teleconnection-based conditional

421   streamflow distributions for the Han River and its sub-watersheds in Korea. *Int. J.*

422   *Climatol.,* **32,** 1466-1474.

423   Li, Y., and S. Yang, 2010: A dynamical index for the East Asian winter monsoon. *J.*

424   *Climate*, **23**, 4255-4262.

425   Lim, Y.-K., Y.-G. Ham, J.-H. Jeong, and J.-S. Kug, 2012: Improvement in simulation of

426   Eurasian winter climate variability with realistic Arctic sea ice condition in an

427   atmospheric GCM. *Env. Res. Lett*., **7,** 044041(6pp) doi:10.1088/1748-9326/7/4/044041.

428   Lim, Y.-K., and H.-D. Kim, 2013: Impact of the dominant large-scale teleconnections on

429   winter temperaturevariability over East Asia. *J. Geophys. Res. Atmos*., **118,** 7835–7848,

430   doi:10.1002/jgrd.50462.

431   Linkin, M. E., and S. Nigam, 2008: The North Pacific Oscillation – West Pacific

432   teleconnection pattern: mature-phase structure and winter impacts. *J. Climate,* **21,**

433   1979-1997.

434   Liu, J., J. A. Curry, H. Wang, M. Song, and R. M. Horton, 2012: Impact of declining Arctic

435   sea ice on winter snowfall. *PNAS,* **109,** 4074-4079.

436 Mo, K. C., and R. E. Livezey, 1986: Tropical-extratropical geopotential height
437   teleconnections during the northern hemisphere winter. *Mon. Wea. Rev*., **114,** 2488-
438   2515.

439 Panagiotopoulos, F., M. Shahgedanova, A. Hannachi, and D. Stephenson, 2005: Observed
440   trends and teleconnections of the Siberian High. *J. Climate*, **18**, 1411-1422.

441 Park, T.-W., C.-H. Ho, and S. Yang, 2011: Relationship between the Arctic Oscillation and
442   cold surges over East Asia. *J. Climate,* **24**, 688-83.

443 Richman, M. B., 1986: Rotation of principal components. *J. Climatol*., **6**, 293–335.

444 Rienecker, M. M., and Coauthors, 2011: MERRA – NASA's Modern-Era Retrospective
445   Analysis for Research Applications. *J. Climate,* **24**, 3624-3648.

446 Sáenz, J., C. Rodríguez-Puebla, J. Fernández, and J. Zubillaga, 2001: Interpretation of
447   interannual winter temperature variations over southwestern Europe. *J. Geophys. Res*.,
448   **106**, D18, 20641-20651.

449 Thompson, D. W. J., and J. M. Wallace, 1998: The Arctic oscillation signature in the
450   wintertime geopotential height and temperature fields. *Geophys. Res. Lett.,* **25(9)**,
451   1297–1300, doi:10.1029/98GL00950.

452 Wang, D., C. Wang, X. Yang, and J. Lu, 2005: Winter Northern Hemisphere surface air
453   temperature variability associated with the Arctic Oscillation and North Atlantic
454   Oscillation. *Geophys. Res. Lett.*, **32**, L16706, doi:10.1029/2005GL022952.

455 Wang, X., C. Wang, W. Zhou, D. Wang, and J. Song, 2011: Teleconnected influence of
456   North Atlantic sea surface temperature on the El Niño onset. *Clim. Dyn*., **37**, 663-676,
457   DOI:10.1007/s00382-010-0833-z.

458 Wallace, J. M., and D. S. Gutzler, 1981: Teleconnections in the geopotential height field

459   during the Northern Hemisphere winter. *Mon. Wea. Rev.,* **109**, 784–812.

460 Washington, R., A. Hodson, E. Isaksson, and O. Macdonald, 2000: Northern hemisphere

461   teleconnection indices and the mass balance of Svalbard glaciers. *Int. J. Climatol*., **20**,

462   473-487.

463 Wu, B., and J. Wang, 2002a: Possible impacts of winter Arctic Oscillation on Siberian high,

464   the East Asian winter monsoon and sea-ice extent. *Advan. Atmos. Sci*., **19**, 297-320.

465 Wu, B., and J. Wang, 2002b: Winter Arctic Oscillation, Siberian high and East Asian

466   winter monsoon. *Geophys. Res. Lett*., **29**, 1897, doi:10.1029/2002GL015373

467 Wu, B., R. Zhang, and R. D'Arrigo, 2006: Distinct modes of the East Asian winter

468   monsoon. *Mon. Wea. Rev*., **134**, 2165-2179.

469

470

471 Table 1 Temporal correlation between the East Asian winter monsoon index (EAWMI),
472   cold surge index (CSI), Siberian high index (SHI), respectively, with teleconnection
473   indices (EA/WR and AO)
474

	EA/WR	AO
EAWMI	-0.59	-0.24
CSI	-0.54	-0.27
SHI	-0.57	-0.21

487

Table 2 Spatial correlation between the pattern associated with the East Asian winter
monsoon index and teleconnection (EA/WR and AO)

490

	T2m	UV850	SLP	U300	Velp
EAWMI .vs. EA/WR	**-0.87**	**-0.86**	**-0.97**	**-0.92**	**-0.86**
EAWMI .vs. AO	**-0.66**	**-0.62**	**-0.56**	**-0.59**	**-0.72**

491

492

Table 3 Spatial correlation between the pattern associated with the cold surge index
and the teleconnection (EA/WR and AO)

495

	T2m	UV850	SLP	U300	Velp
CSI .vs. EA/WR	**-0.85**	**-0.84**	**-0.95**	**-0.92**	**-0.91**
CSI .vs. AO	**-0.60**	**-0.57**	**-0.54**	**-0.60**	**-0.68**

496

497

Table 4 Spatial correlation between the pattern associated with the Siberian high
index and the teleconnection (EA/WR and AO)

500

	T2m	UV850	SLP	U300	Velp
SHI .vs. EA/WR	**-0.92**	**-0.69**	**-0.97**	**-0.95**	**-0.71**
SHI .vs. AO	**-0.74**	**-0.62**	**-0.53**	**-0.65**	**-0.65**

501

502
503
504
505
506
507
508
509
510
511
512
513
514
515
516
517
518
519
520
521
522
523
524
525
526
527
528
529
530
531
532
533
534
535
536
537
538
539
540
541
542
543
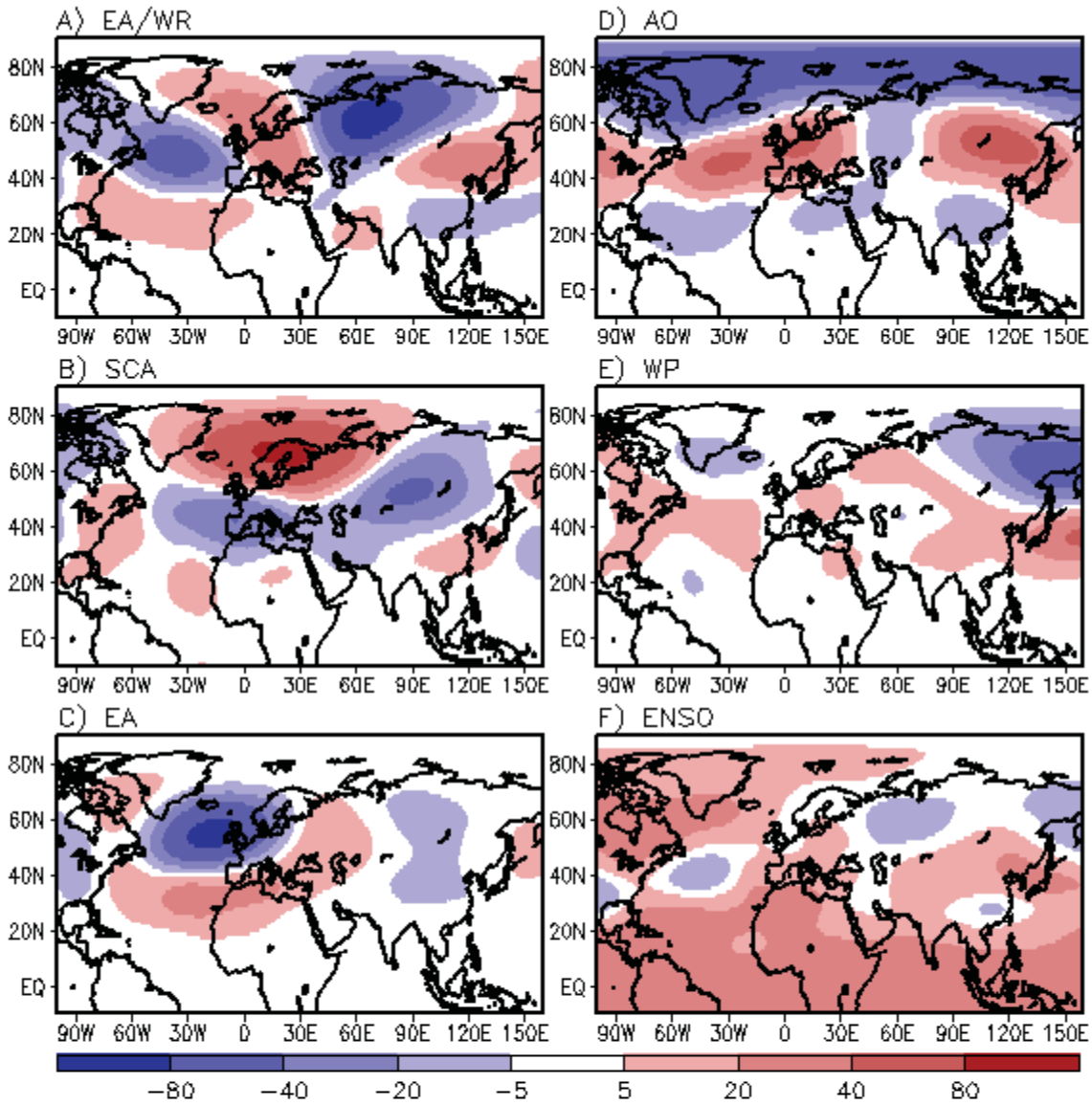
Figure 1. The non-normalized rotated empirical orthogonal functions (REOFs) of the monthly 250 hPa height [m] archived from a MERRA reanalysis. The analysis period included the last 34 winters from December–February (DJF) 1979/80 through DJF 2012/13. The left panel represents the distribution of European teleconnections (East Atlantic/West Russia, Scandinavia, and East Atlantic) whereas the right panel represents the Arctic Oscillation, the Western Pacific, and the El-Niño Southern Oscillation.
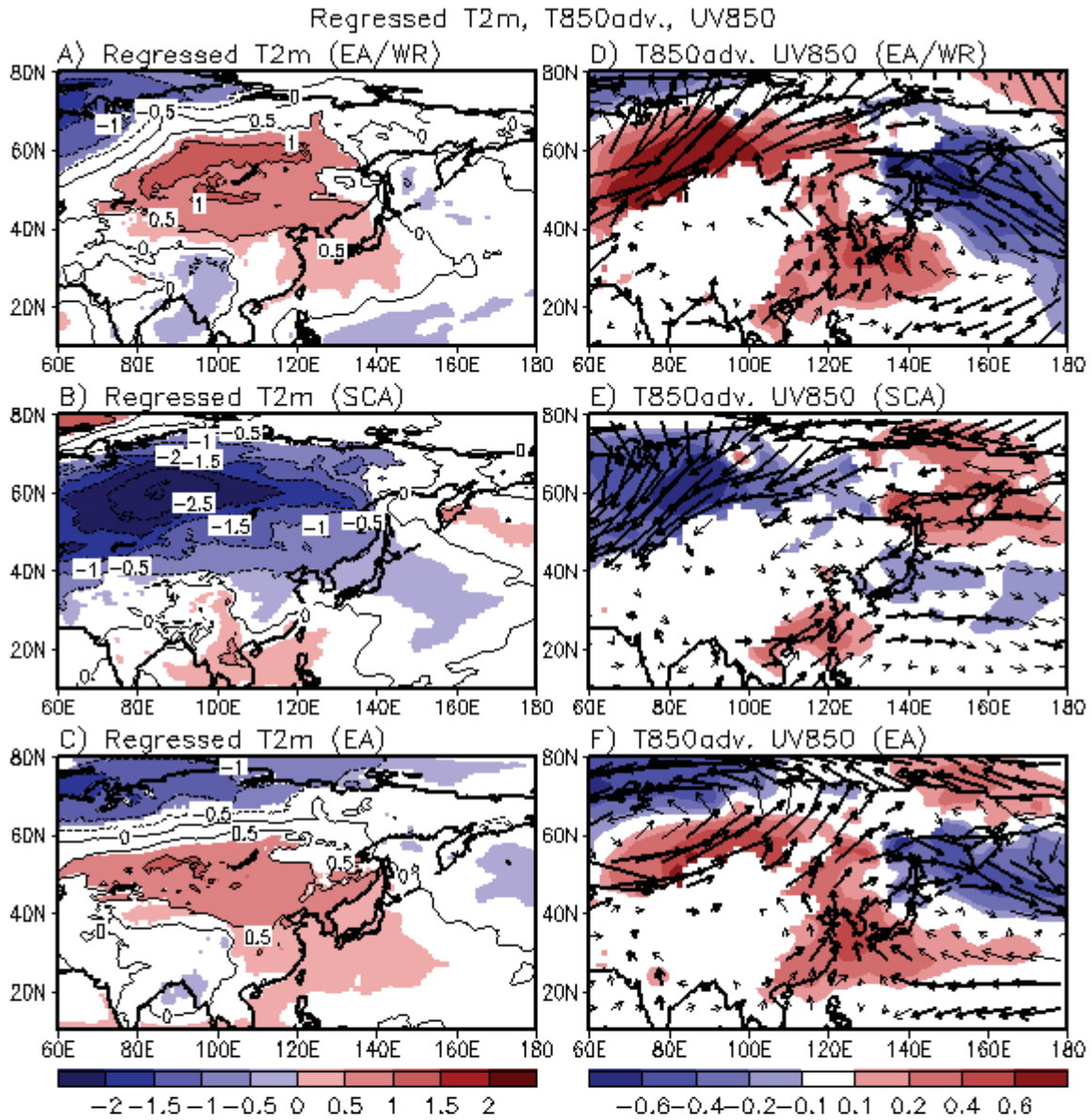
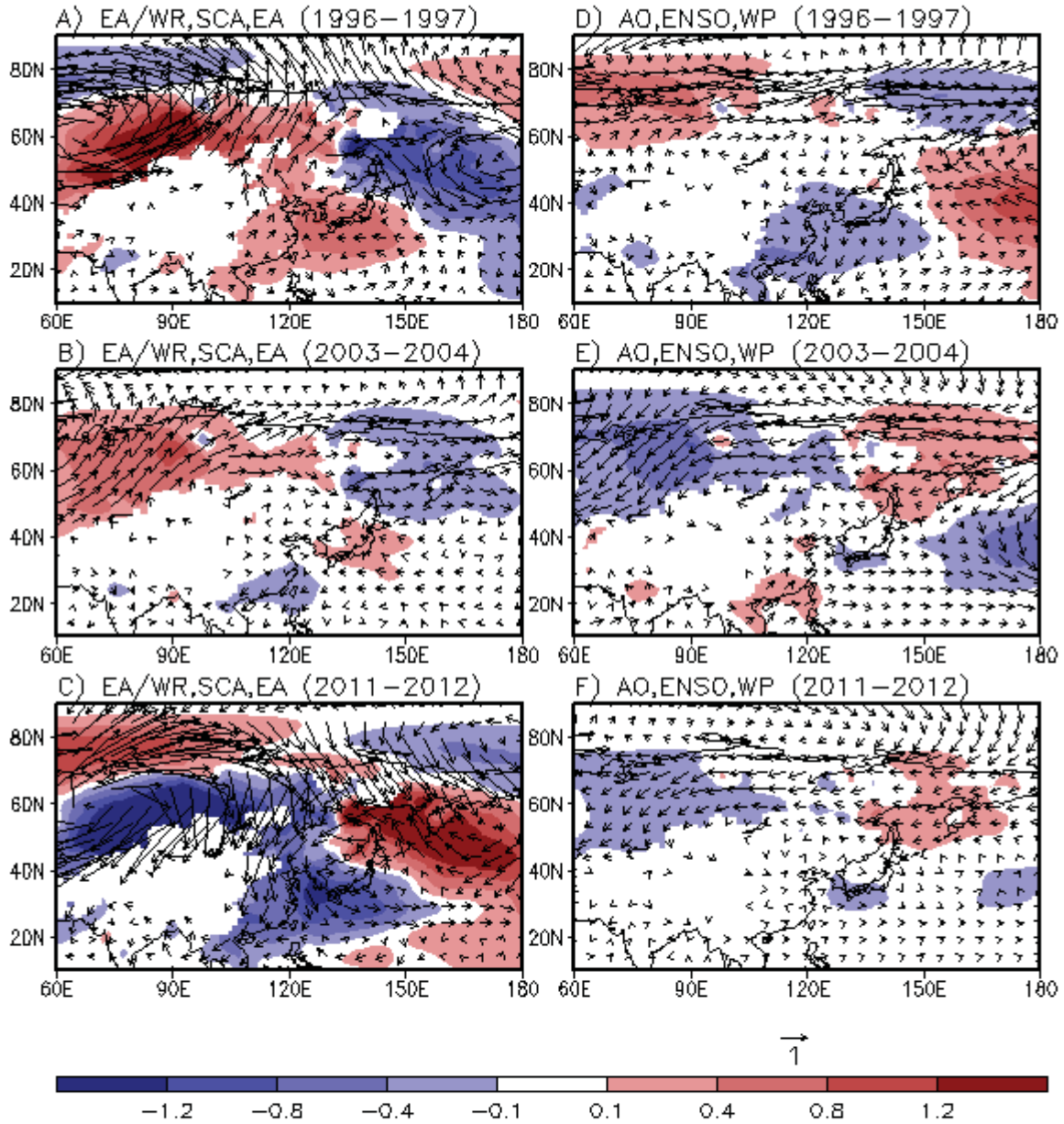**Figure 2**. Distribution of the 2 meter air temperature anomalies (left panel) [K] and the atmospheric circulation and advective temperature change ($-V_{Tel} \cdot \nabla T_{Cli}$) [K day^{-1}] at 850 hPa (right panel) associated with one standard deviation in each European teleconnection time series based on linear regression. Shaded regions are where the anomaly values are statistically significant at 10%. Wind vectors statistically significant at 10% level are plotted as thick lines. V_{Tel} denotes the regressed horizontal winds, and T_{Cli} represents the climatological monthly temperatures. Note that the high-elevation region in continental Asia such as western China and the Tibetan area is treated as missing in the right panel.

588

589

590
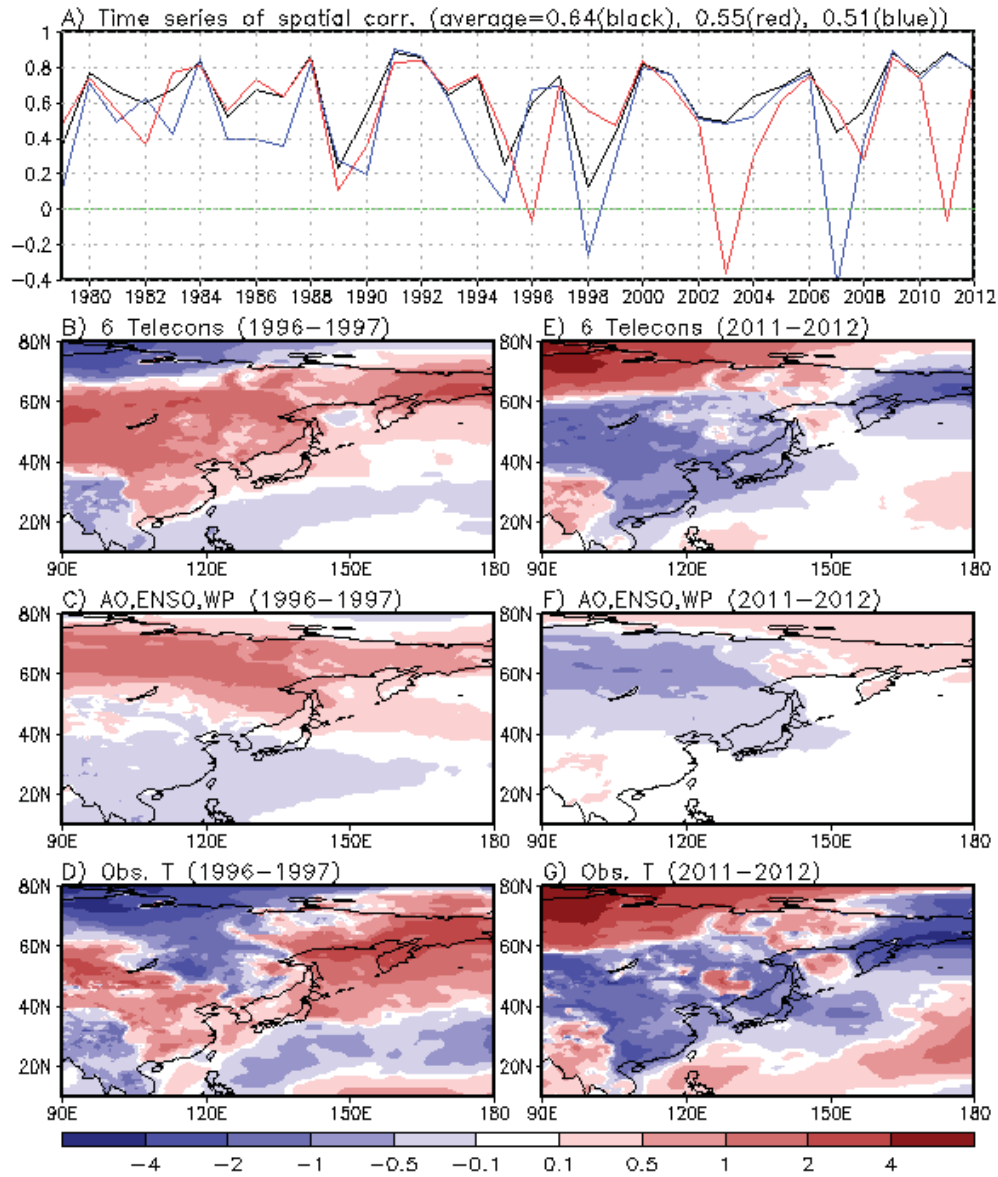
Figure 3. Upper: Time series of the spatial correlation coefficients between observed temperature anomalies (temporal anomalies) and the reconstructed temperatures comprised of both AWE and ESE impacts (black), ESE impact (blue), and AWE impact (red), respectively, for the geographic domain shown in the lower panels. B) and E) represent the winter temperature anomalies by the combined effect of AWE and ESE for 1996–97 (B) and 2011–12 (E), respectively. C) and F) are the same as B) and E) but for the anomalies caused by the impact of AWE. Observed temperature anomaly distributions for those years are shown in D) and G) for comparison.

616

Figure 4. Distribution of the atmospheric circulation and advective temperature change $(-V_{Tel} \cdot \nabla T_{Cli})$ [K day^{-1}] at 850 hPa caused by the impact of ESE (left panel) and AWE (right panel) for the three selected winter cases (1996–97, 2003–04, and 2011–12). Note that the high-elevation region in continental Asia such as western China and the Tibetan area is treated as missing.

662

663

664

665

666

667

668

669

670
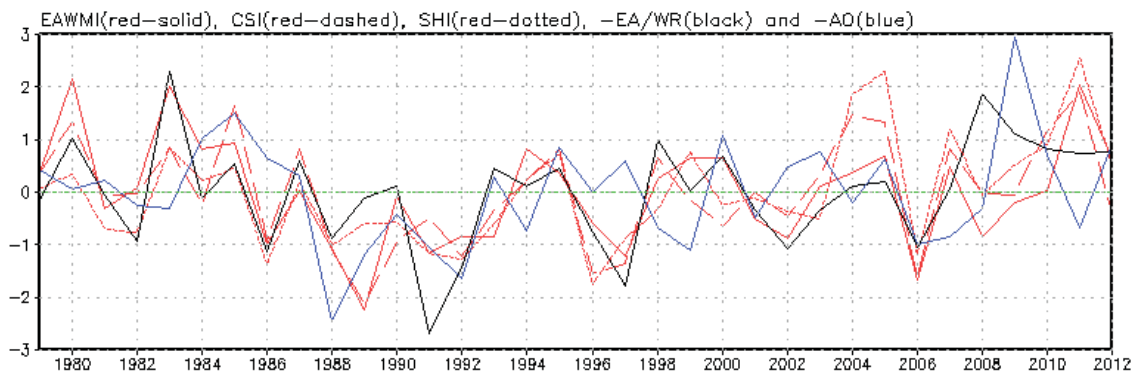
671 **Figure 5**. Interannual variation in normalized EAWMI, CSI, SHI, –EA/WR, and –AO.
672 They are denoted by red-solid, red-dashed, red-dotted, black solid, and blue solid line,
673 respectively.

674

675
676
677
678
679
680
681
682
683
684
685
686
687
688
689
690
691
692
693
694
695
696
697
698
699
700
701
702
703
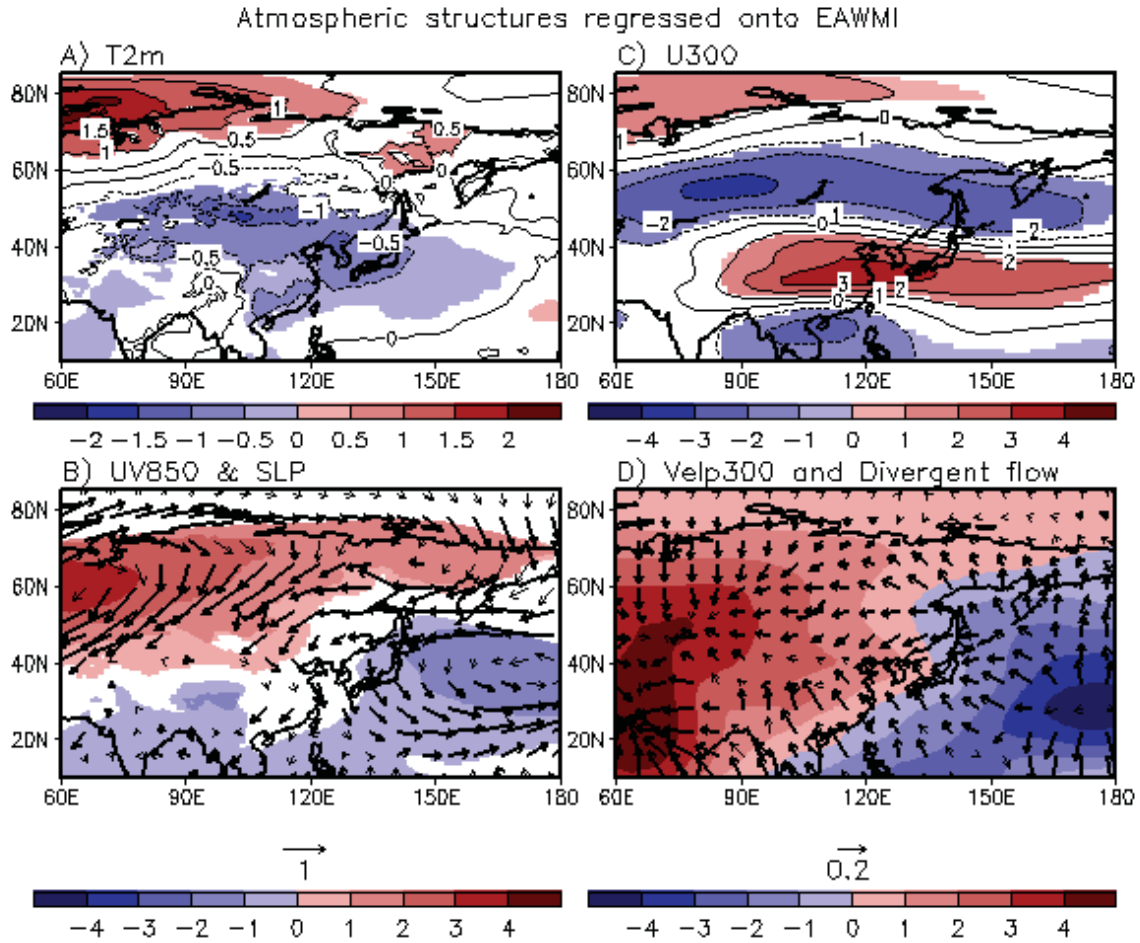
704 **Figure 6**. Horizontal distributions of atmospheric variables regressed onto EAWMI. Except
705 velocity potential [1.0e+5 m^2s^{-1}] on the lower-right panel, the shaded area indicates where
706 the values are significant at the 10% level. Thick arrows on the bottom panel (B and D)
707 indicate vectors significant at the10% level.
708

709
710
711
712
...
755
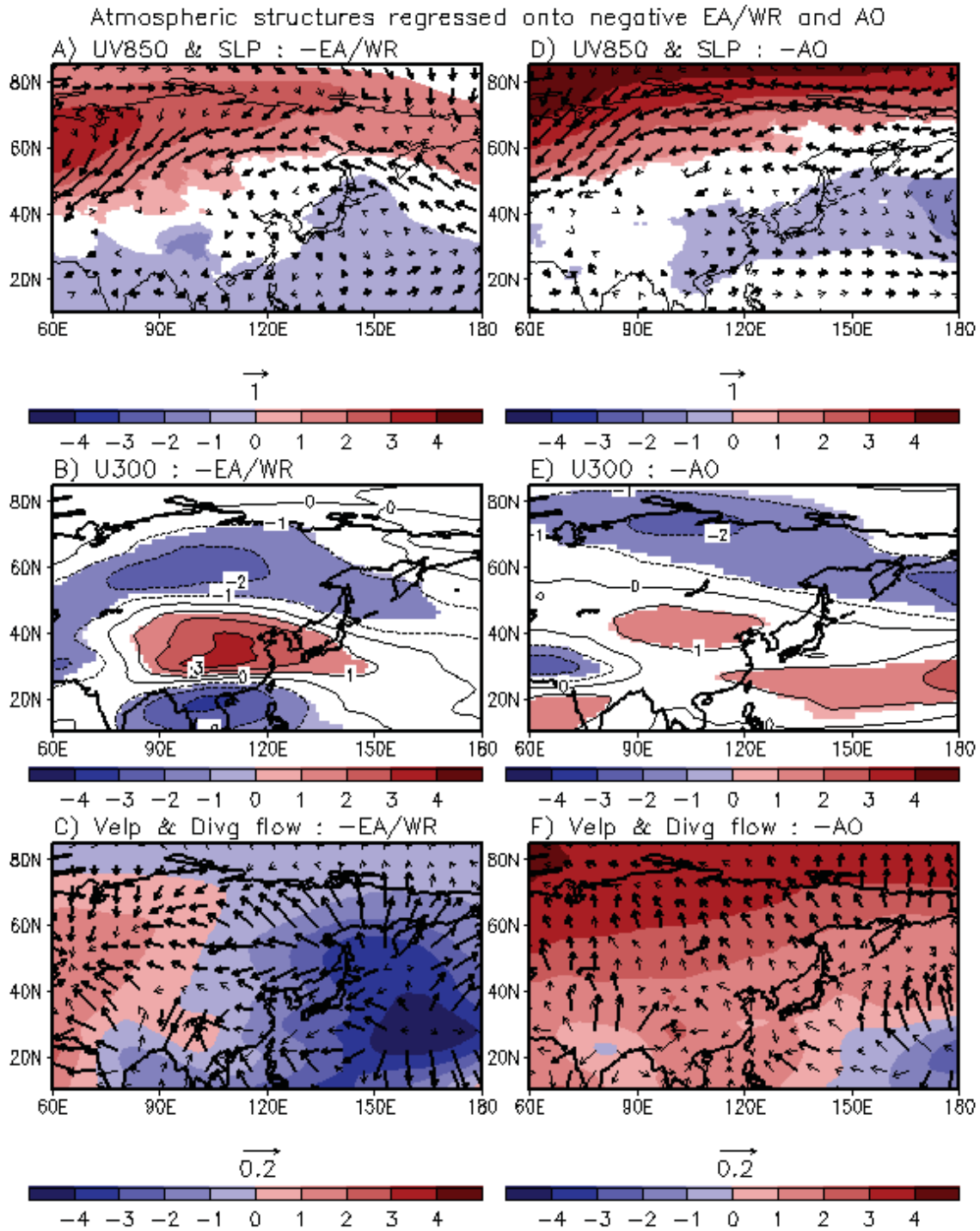
Figure 7. Horizontal distributions of atmospheric variables regressed onto –EA/WR (left) and –AO (right). Except velocity potential [1.0e+5 m^2s^{-1}] on the bottom panel (C and F), shaded area indicates where values are significant at the 10% level. Thick arrows on the top (A and D) and bottom panel (C and F) indicate vectors significant at the 10% level.
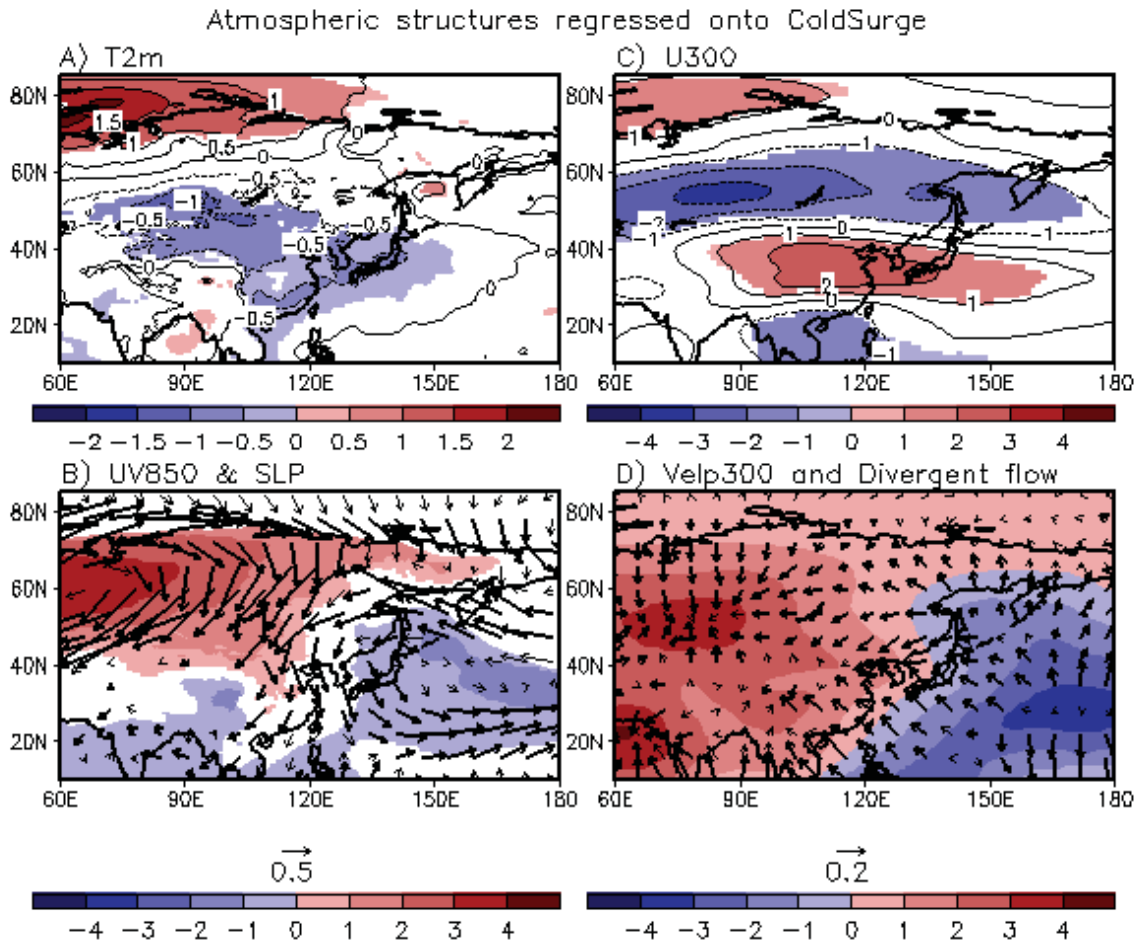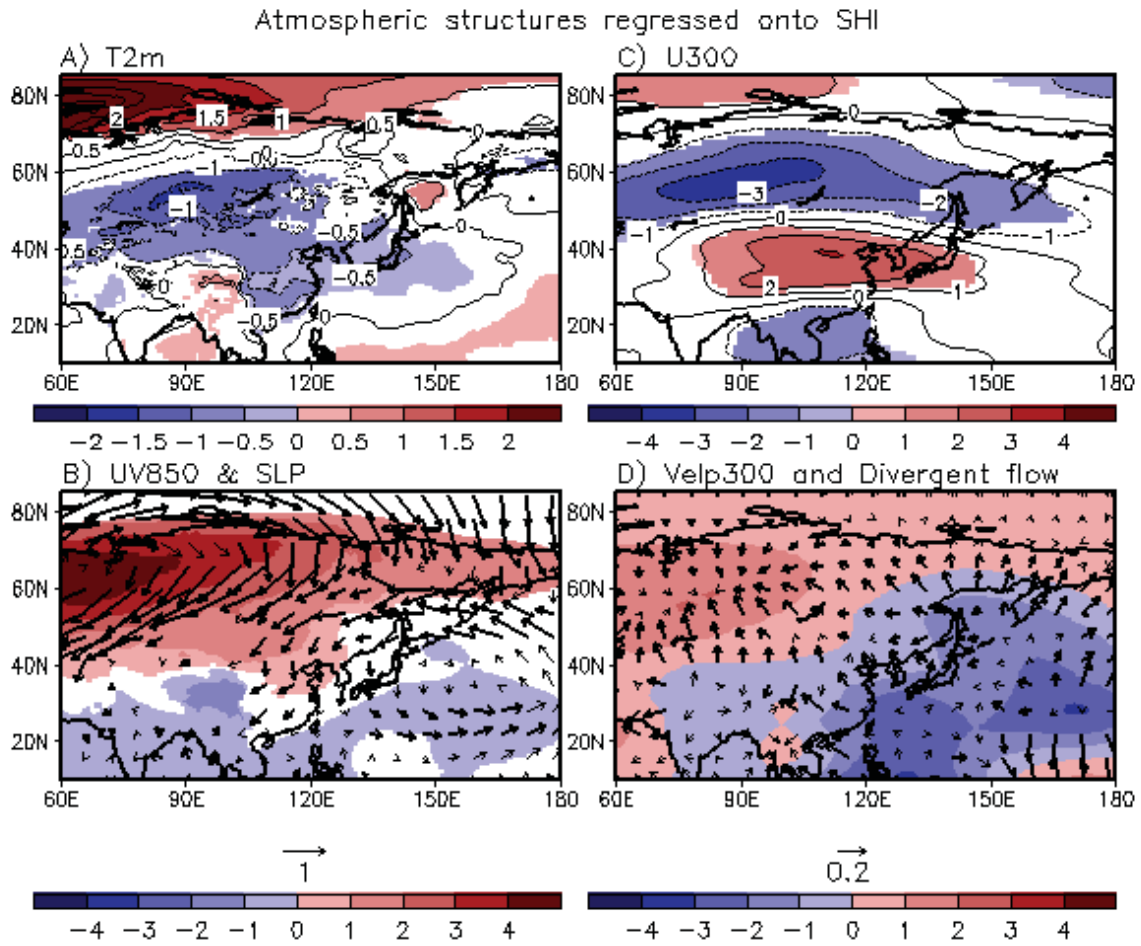
Figure 8. Same as Figure 6 but for regression onto CSI.

Figure 9. Same as Figure 6 but for regression onto SHI.